International Journal of Concrete Structures and Materials
Vol.11, No.2, pp.315–325, June 2017
DOI 10.1007/s40069-017-0195-6
ISSN 1976-0485 / eISSN 2234-1315

Effect of Fiber Hybridization on Durability Related Properties of Ultra-High Performance Concrete

Piotr Smarzewski[1),*], and Danuta Barnat-Hunek[2)]

(Received March 22, 2016, Accepted February 6, 2017, Published online May 18, 2017)

Abstract: The purpose of the paper is to determine the influence of two widely used steel fibers and polypropylene fibers on the sulphate crystallization resistance, freeze–thaw resistance and surface wettability of ultra-high performance concrete (UHPC). Tests were carried out on cubes and cylinders of plain UHPC and fiber reinforced UHPC with varying contents ranging from 0.25 to 1% steel fibers and/or polypropylene fibers. Extensive data from the salt resistance test, frost resistance test, dynamic modulus of elasticity test before and after freezing-thawing, as well as the contact angle test were recorded and analyzed. Fiber hybridization relatively increased the resistance to salt crystallization and freeze–thaw resistance of UHPC in comparison with a single type of fiber in UHPC at the same fiber volume fraction. The experimental results indicate that hybrid fibers can significantly improve the adhesion properties and reduce the wettability of the UHPC surface.

Keywords: ultra-high performance concrete, steel fibers, polypropylene fibers, salt resistance, frost resistance, contact angle, surface free energy.

1. Introduction

Ultra-high performance concrete is often used in underground waterproof projects, roads, bridges and seismic structures in harsh environmental conditions. The material is characterized by high strength, low absorbability, low water permeability and high freeze resistance, which results in high durability (Smarzewski and Barnat-Hunek 2013; Li and Liu 2016; Kang et al. 2016). This material has a low porosity and might be filled with a gaseous phase or liquid phase. The liquid phase contains water and various types of pollutants including salts, which penetrate the concrete through the interconnected pores (Koniorczyk et al. 2013). Therefore, knowledge about the wettability, absorptivity, frost resistance and salt resistance of a given UHPC formulation is extremely important when considering its durability. The frost resistance of fiber reinforced concrete is affected by its porosity, type of aggregate, fiber characteristics and environmental conditions; hence, the frost resistance of ultra-high performance concrete mixtures has been investigated by some researchers (Yun and Wu 2011). Chemrouk and Hamrat have shown that a water/cement ratio below 0.4 reduces the penetration of chlorides, decreases the risks of concrete spalling and rebar corrosion in reinforced concrete structures (Chemrouk and Hamrat 2002). UHPC is characterised by a maximum aggregate size of 8 mm. The water/binder ratio is frequently below 0.25 and highly reactive silica fume must be added to the mix. Workability can be ensured by applying large amounts of superplasticizer (2009). Fibers are added to the matrix as reinforcement to control cracking and to increase material ductility (Dinh et al. 2016; Abdallah et al. 2016; Bencardino et al. 2010; Abou El-Mal et al. 2015; Sorensen et al. 2014). The cracks in concrete generally occur over time due to a number of reasons. Cracks weaken the waterproofing capabilities and expose the microstructure to moisture, bromine, chloride and sulphates (Köksal et al. 2008; Song et al. 2005; Sivakumar and Santhanam 2007; Toutanji 1999). Thus, improving concrete properties is an important aim in concrete science (Nili and Afroughsabet 2012). Cracks occur in different sizes and at different stages of concrete exploitation; consequently, the use of different fibers with various lengths and varied characteristics are a good way to solve this problem. The interaction between the fibers and the concrete is more advantageous when two types of fibers are used (Yao et al. 2003; Dawood and Ramli 2010; Yang 2011). Concrete deterioration is associated with destructive chemical attacks and the impact of freezing and thawing (Chemrouk 2015; Bondar et al. 2015). Another factor that affects concrete durability is resistance to the ingress of aggressive ions (Afroughsabet and Ozbakkaloglu 2015). The most frequent sulphate salts are calcium sulphate (Ca_2SO_4), sodium sulphate (Na_2SO_4), potassium sulphate

[1)]Department of Structural Engineering, Faculty of Civil Engineering and Architecture, Lublin University of Technology, 40 Nadbystrzycka Str., 20-618 Lublin, Poland.
*Corresponding Author; E-mail: p.smarzewski@pollub.pl
[2)]Department of Construction, Faculty of Civil Engineering and Architecture, Lublin University of Technology, 40 Nadbystrzycka Str., 20-618 Lublin, Poland.

(K_2SO_4) and magnesium sulphate ($MgSO_4$), the most aggressive salts of which are sodium sulphate and potassium sulphate (Chemrouk 2015). Not only does the growth of salt crystals in concrete pores generate stress leading to damage, but the growth of ice is another reason for concrete quality deterioration. Scherer (Scherer 1999) proved that the crystallization pressure of salt is low in large pores; on the other hand, the impact of freeze–thaw cycles is more evident in the small pores of UHPC. Nevertheless, few investigations of freezing-thawing resistance can be found for fiber reinforced concrete (Miao et al. 2002; Colombo et al. 2015). In practice, concrete degradation mechanisms are the combined results of mechanical stress, physical and chemical attacks (Miao et al. 2002). The resistance of concrete to freezing and thawing depends on the degree of saturation, system of pores, permeability and the water/binder ratio. High freezing-thawing resistance depends on low permeability and a low water/binder ratio (Colombo et al. 2015). For concrete with a high freezing-thawing resistance, the distance from the hydrated cement paste to an air void cannot exceed 0.2 mm. In addition, very small pores with diameters less than 0.3 mm are desirable (Yang et al. 2015). High strength concrete with a very low water/binder ratio generally has a low capillary porosity. Hence, the amount of water able to freeze is low enough and concrete can be damaged by frost action after long and continuous exposure to water (Guse and Hilsdorf 1998). However, the doubts regarding the frost resistance of high performance concretes have not been entirely removed (2009). The expansive reactions in concrete are related to the sulphates contained in ground water, sea water, soils and sewage. Sulphate attack is associated with the groundwater environment and the discharge of industrial wastewater (Çavdar 2014). Sulphate ions during penetration of the concrete may react with calcium hydroxide or with calcium aluminate hydrates. Severe damage, and in the end complete disintegration occur if sulphate solutions penetrate the hardened concrete. UHPC are often exposed to aggressive impacts from the environment, thus they must have high resistance to chemical corrosion, frost corrosion, weathering or the influence of aggressive water. In paper (Çavdar 2014), the flexural strength, compressive strength and modulus of dynamic elasticity of fiber reinforced mortar samples after 100 freeze–thaw cycles were reduced. Frost and salt resistance are considered to be significant features in evaluating concrete durability.

The purpose of this article is to determine the influence of steel and polypropylene fibers on the freeze–thaw resistance, sulphate crystallization resistance and surface free energy of ultra-high performance concrete.

2. Experimental Methods

2.1 Materials

In the mixes Portland cement CEM I 52.5 N-HSR/NA, condensed silica fume, two types of coarse aggregates: granodiorite and granite, quartz sand, water, superplasticizer and two types of fibers: steel (SF) and polypropylene (PF), were used. Tests on the cements were carried out according to PN-EN 197-1:2012. The properties of the cement are shown in Table 1.

Based on PN-EN 933-1:2000, the particle size distribution for coarse and fine aggregate was performed. In order to attain the same workability, a highly effective superplasticizer with a density of 1.065 g/cm3 at 20 °C, based on polycarboxylate ethers intended to create a self-compacting concrete, was used. The SF properties are the following: hooked-end with density 7.8 g/cm^3, length 50 mm, diameter 1 mm, modulus of elasticity 200 GPa, tensile strength 1100 MPa and the PF characteristics are: density 0.9 g/cm^3, length 12 mm, diameter 25 μm, modulus of elasticity 3.5 GPa, tensile strength 350 MPa. The mixes were prepared using: cement—670.5 kg/m^3, granodiorite aggregate 2/8 mm (in C1, SC, SPC1 mixes) or granite aggregate 2/8 mm—990 kg/m^3 (in SPC2, SPC3, PC, C2 mixes), quartz sand 0.1/2 mm—500 kg/m^3, water—178 l/m^3, silica fume—74.5 kg/m^3, and superplasticizer—20 l/m^3. The quantities of SF and PF were varied. The purpose of using two types of aggregates was to determine their effect on the fracture parameters of UHPC (Smarzewski and Barnat-Hunek 2015). The abbreviations of the concrete mixes, quantities of steel and polypropylene fibers and types of coarse aggregate are shown in Table 2.

The mixtures were prepared using a concrete mixer with a capacity of 100 l. At the beginning of mixing the coarse aggregate and sand were homogenized with a half of the amount of water. Subsequently, cement, silica fume, the remaining water were added and finally the superplasticizer. After the concrete components had been thoroughly mixed, steel and polypropylene fibers were added by hand to obtain a homogeneous and workable consistency.

Samples were formed directly after all the components had been mixed. Moulds coated with anti-adhesive oil were filled with a concrete batch and compacted on a vibrating table. The cubical samples were compacted in one layer, while the cylindrical samples were done in two layers. After compacting, the samples were covered with foil to minimize the loss of moisture. All the samples were stored at a temperature of about 23 °C until the time to remove them from the moulds after 24 h, then they were placed in a water tank for 7 days to cure. Over the next few days, until completion of the test—after 28 days, the samples remained in air-dry conditions.

2.2 Test Methods

Tests were carried out on cube samples and cylindrical samples. The physical properties of the concrete were described in paper (Barnat-Hunek and Smarzewski 2016). The dynamic modulus of elasticity before and after the cyclic freezing-thawing test and the salt crystallization resistance test was measured.

2.2.1 Resistance to salt crystallization

The resistance to salt crystallization was tested according to standard EN 12370:2001. Six cubes from each mix were used for the test. The dimensions of the samples were the following: 100 × 100 × 100 mm. The samples were immersed in a 14% solution of sodium sulphate dehydrate for the period of 2 h after drying and weighing, Fig. 1.

Table 1 Cement properties.

Cement properties	Unit	Value
Specific surface area	cm^2/g	4433
Water demand	%	30
Commencement of bonding	min	120
End of bonding	min	180
Volume stability	min	2
Compressive strength at 2 days	MPa	27.7
28 days	MPa	57.1
Tensile strength at 2 days	MPa	5.3
28 days	MPa	8.2

Table 2 Variable components of concrete mixtures.

Type of UHPC	Percentage of fibers (%)/mass (g/cm^3)		Type of coarse aggregate 2/8 mm
	Steel fibers SF	Polypropylene fibers PF	
C1	–	–	Granodiorite
SC	1/7.8	–	Granodiorite
SPC1	0.75/5.85	0.25/0.23	Granodiorite
SPC2	0.5/3.9	0.5/0.45	Granite
SPC3	0.25/1.95	0.75/0.68	Granite
PC	–	1/0.9	Granite
C2	–	–	Granite

Then they were dried in conditions of a progressive temperature increase until 105 °C for about 10 h, maintaining a high relative moisture at the initial stage of drying. Afterwards, the samples were saturated in sodium sulphate again. The cycle of saturation and drying was repeated 15 times. Then the samples were stored in water for 24 h. After saturation the specimens were washed, dried and weighed. The obtained results are presented in percent as the relative difference in mass in relation to the initial mass of the sample and the number of cycles till concrete surface degradation, which meant a lack of resistance to salt crystallization.

2.2.2 Frost Resistance Test

Frost resistance was determined using the direct method according to EN 12012:2007 and EN 13581:2004. Six cylindrical samples 150 mm in diameter and of a height of 300 mm from each mix were subjected to 180 cycles of freezing and thawing (F-T). These samples were placed in a freezing chamber in which the temperature control range is −30 to 60 °C (Fig. 2). The cyclic freeze–thaw scheme is illustrated in Fig. 2. At the beginning the temperature was kept constant at 20 °C for 1 h to eliminate an initial temperature difference between the samples and the chamber. The rate of freezing in water ranged from 20 to −20 °C for 6 h. In turn, the rate of thawing in water ranged from −20 to 20 °C for 6 h. One F–T cycle duration was 12 h. After 90 days all the samples were dried to a constant mass, then the mass loss, dynamic modulus of elasticity and contact angle were determined. During the measurements the samples were stored under similar conditions.

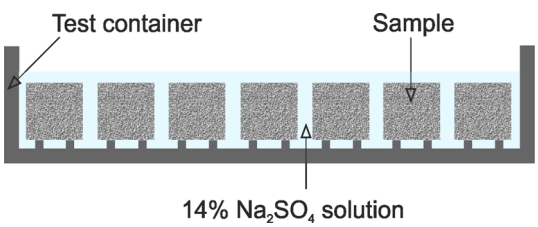

Fig. 1 Experimental set-up of UHPC resistance to sodium sulphate crystallization test.

2.2.3 Dynamic Modulus of Elasticity

Dynamic modulus of elasticity testing was performed on six cylinders 150 mm in diameter and of a height of 300 mm, from each mix before and after the frost resistance test. Determination of the dynamic modulus of elasticity was performed based on the resonant frequency of vibration of a sample generated by an impact and sensed by an accelerometer. The test was conducted based on ASTM C666 and ASTM C215. In the experiment, an accelerometer was installed on a cylindrical sample and was attached to the battery operated instrument, Fig. 3. A hardened steel ball was used as the impactor. The steel ball struck the top surface of the cylindrical specimen, then the apparatus

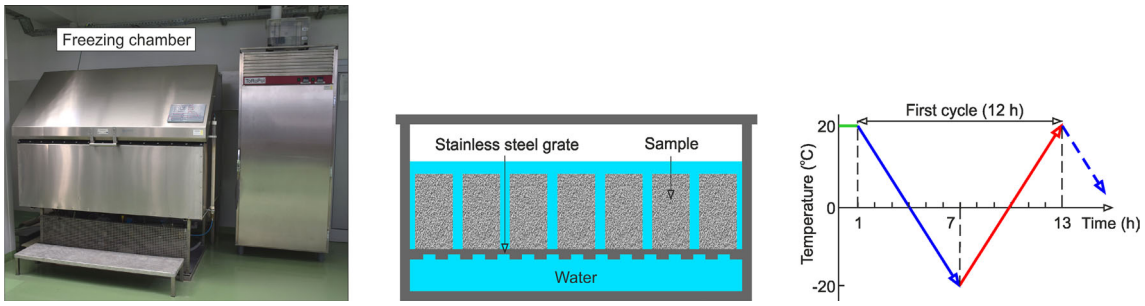

Fig. 2 Experimental set-up, schematic diagram, and cyclic temperature scheme for freeze–thaw test.

computed the maximum amplitude. The transverse (flexural) resonance is valid to determine the durability of UHPC by testing the degradation of concrete after freezing-thawing cycles and aggressive environments on concrete samples.

The dynamic modulus, E_{DM} (GPa), was calculated from the formula:

$$E_{DM} = 4\rho L^2 n^2 \tag{1}$$

where ρ—density (kg/m^3), L—specimen length (m), n—frequency (kHz).

2.2.4 Contact Angle and Surface Free Energy

Contact angle measurements were conducted to calculate the surface free energy (SFE). Measurement of the contact angle of a distilled water drop was carried out on a research stand consisting of a goniometer integrated with a camera for taking photos of a drop put onto the sample surface, Fig. 4.

Distilled water drops of 2 mm^3 were deposited by means of a syringe. Due to the heterogeneity of the material surface, six drops were put on each sample. The measurements were carried out at the time of drop application and after 35 min. Measurements were performed before and after the frost resistance test of 180 cycles of freezing-thawing in order to verify change in the adhesive properties and wettability of UHPC. Measurement of the contact angle of a distilled water drop is shown in Fig. 5.

The Neumann model was applied to calculate SFE. The total SFE for the distilled water, $\gamma_w = 72.8$ mJ/m^2, was adopted. In the Neumann model the following equation for calculating SFE was used (Barnat-Hunek and Smarzewski 2016):

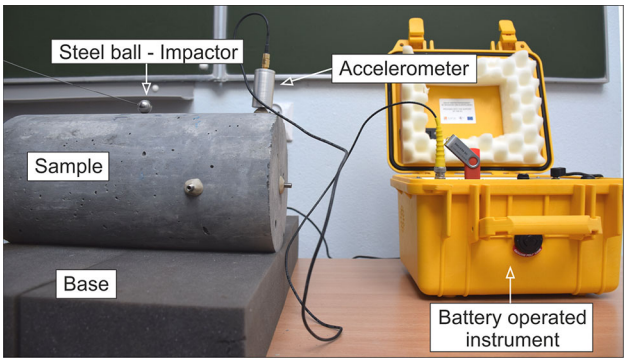

Fig. 3 Set-up of dynamic modulus of elasticity test for cylindrical sample.

$$\left(\frac{\gamma_w}{\gamma_s}\right)^{1/2} = \frac{e^{-\frac{1}{8000}(\gamma_s-\gamma_w)^2}}{(\cos\theta_w + 1)} \tag{2}$$

where γ_s—SFE value for UHPC, θ_w—distilled water contact angle.

3. Results and Discussion

3.1 Physical and Mechanical Properties

A higher air content has a detrimental effect on the durability related properties of UHPC. Depending on the UHPC components, the air content ranges from 0.3 to 6% by volume of mixture (Wille et al. 2011; Wang and Gao 2016). The air content in UHPC was 1% owing to using superplasticizer in the amount of 20 kg/m^3, and a water/binder (w/b) ratio equal to 0.17 (Pierard and Cauberg 2009). A higher w/b ratio and higher superplasticizer dosage led to an increased air content (Abbas et al. 2016). On the other hand, special mixing technology under lowered air pressure reduces the air content (Dils and De Schutter 2015). Moreover, the addition of steel fiber decreased the entrapped air content of fresh UHPC mixtures when a high dosage of superplasticizer was used (Wang and Gao 2016). Less workable concrete contains more entrapped air which cannot escape from the mass because of the high viscosity of the mixture. Poor workability leads to a higher content of air in the cavities and pores of the capillaries which have an important impact on the mechanical properties and the durability properties of the concrete (Dils et al. 2013). When the capillary porosity decreases, a small amount of water is absorbed and saturation does not occur so easily. This gives a higher resistance to freeze–thaw cycles, and penetration of chlorides and sulphates (Dils et al. 2013; Aïtcin 2003). The mean values of UHPC properties shown in Table 3 are based on papers (Smarzewski and Barnat-Hunek 2015; Barnat-Hunek and Smarzewski 2016).

A greater amount of polypropylene fibers (PF) causes a decrease in density. The pore volume increased the number of micro-cracks which are formed in the cement mortar due to a poor transition zone and weaker adhesion between PF and the cement matrix. This affected an increase in concrete absorptivity. The test results for polypropylene fiber reinforced UHPC indicate the negative impact of PF on decreasing the water absorption of concrete. An inverse relationship for UHPC with a high content of steel fibers

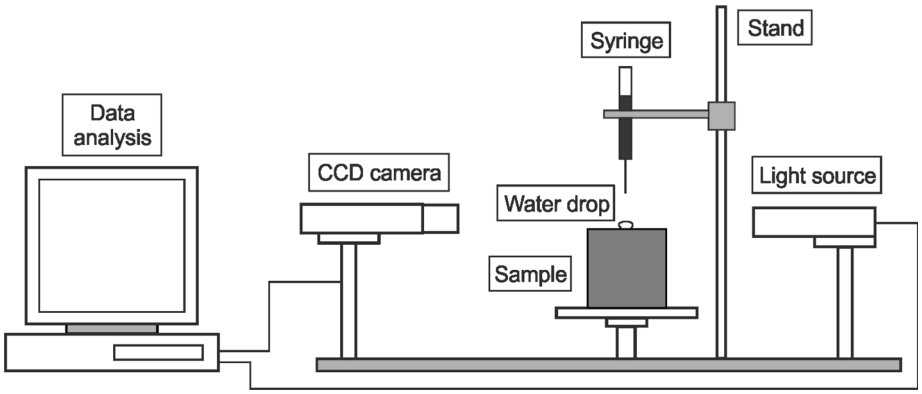

Fig. 4 Equipment used in contact angle measurement.

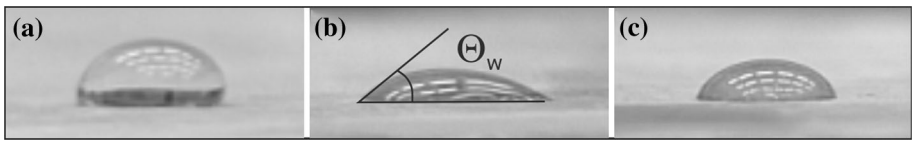

Fig. 5 Measurement of contact angle with distilled water (θ_w) for UHPC with steel fiber (0.25%) and polypropylene fiber (0.75%), with granite aggregate: **a** before frost resistance test, $t = 0$ min, **b** before frost resistance test, $t = 35$ min, **c** after frost resistance test, $t = 0$ min.

Table 3 UHPC properties.

Property of UHPC	C1	SC	SPC1	SPC2	SPC3	PC	C2
Apparent density (g/cm^3)	2.57	2.61	2.51	2.45	2.36	2.30	2.40
Absorptivity (%)	0.60	0.54	0.69	0.78	0.95	1.07	0.75
Compressive strength (MPa)	151.0	154.9	144.7	133.9	122.3	94.6	129.5
Splitting tensile strength (MPa)	8.9	13.8	13.5	10.0	9.3	7.6	6.8
Modulus of elasticity (GPa)	38.37	39.74	34.27	32.45	29.60	29.42	32.55

(SF) is observed. A larger amount of SF increases the strength of UHPC. The compressive strength of PF reinforced UHPC is significantly lower than concrete without fibers, and with granite aggregate. The reason for the decrease in the compressive strength is probably that dispersion at 1% PF volume was difficult, caused poor workability, and incomplete consolidation of UHPC. A decrease in compressive strength by adding polypropylene fibers was also observed by other researchers (Khitab et al. 2013; Afroughsabet et al. 2016).

3.2 Resistance to Salt Crystallization

The examined cube samples were visually monitored after 15 cycles of sulphate exposure. No deterioration was observed on the cube surfaces. A loss in mass was observed in the samples with a high SF content. On the other hand, there was an increase in weight in the samples without fibers, and with a PF content at least 0.5% (Fig. 6).

Only in concretes with the high contents of steel fiber (1 and 0.75%) was a slight decrease in the mass of the concrete (0.14 and 0.05% respectively) observed. In this study, the water absorptivity corresponds to the increase in mass in the sample after the salt crystallization test (Fig. 7).

The polynomial trend was characterized by correlation coefficient $R^2 = 0.7822$ and relatively low errors in the intercept. A higher increase in mass after the salt crystallization test was observed in the concretes with 1 and 0.75% PF, with the granite aggregate and with the highest absorptivity. This is due to the greater amount of free pores which were filled by salt.

3.3 Frost Resistance Test

There are many tests that can be used to determine the frost resistance of UHPC. How many cycles of freezing and thawing should be performed to consider it resistant to freezing and thawing remains an open question. ASTM C 666 recommends procedure A (freezing and

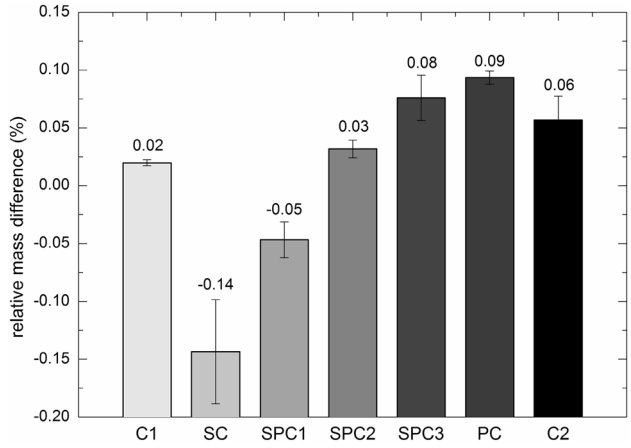

Fig. 6 Relative increase/decrease in sample weight after salt crystallization test.

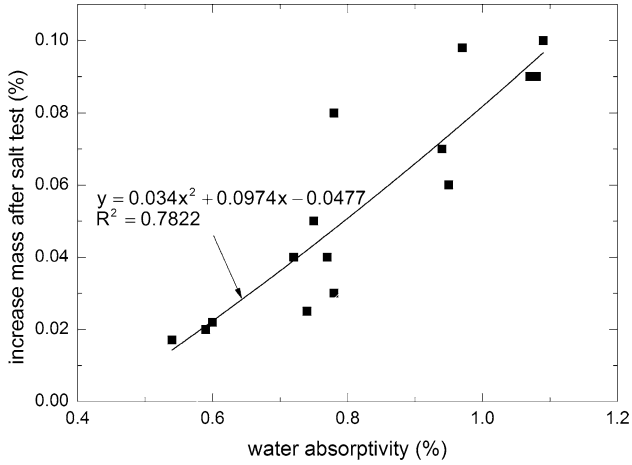

Fig. 7 Relationship between water absorptivity and increase in mass after salt crystallization test.

thawing in water) or procedure B (freezing in air and thawing in water) to determine freeze–thaw resistance. In both procedures, the number of F–T cycles is equal to 300 and mostly adopts a cycle of 2 h of freezing and 2 h of thawing. The ASTM C 666 sequence is very high and it does not represent well natural freeze–thaw exposure, nevertheless, this method is commonly used. In this research the number of cycles was reduced to 180 and the duration of a freezing-thawing cycle was extended to 12 h.

The addition of steel fibers significantly increased UHPC degradation after 180 freezing-thawing cycles. The steel fibers can change the failure mode of samples subjected to cyclic freezing and thawing. After the experiment, we observed cracks on the concrete surface and corrosion of the steel fibres in the samples with the 1% SF content, see Fig. 8.

More cracks and voids can be observed in the concrete with SF in the amounts of 1% (SC) and 0.75% (SPC1) with the granodiorite aggregate which resulted in a higher mass loss. In other cases, the swelling pressure of ice was sufficient to cause disruptive micro-cracks that during the process became macro-cracks which extended throughout the affected concrete. The average mass loss of the samples with error bars is shown in Fig. 9.

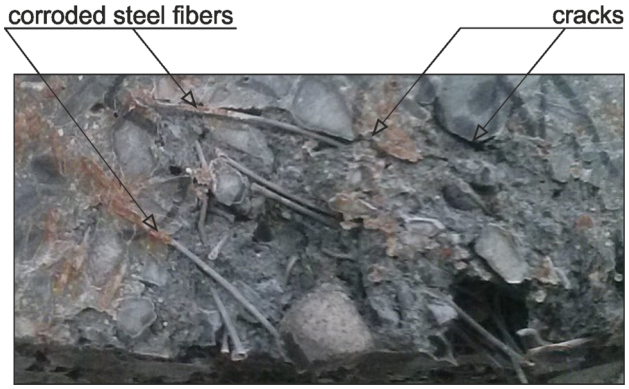

Fig. 8 Failure mode of concrete sample with 1% SF content after freeze–thaw resistance test.

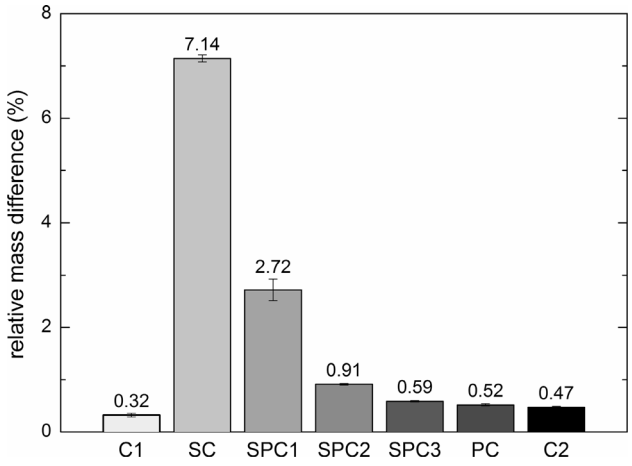

Fig. 9 Relative decrease in mass after freeze–thaw resistance test.

The greatest mass loss was demonstrated by the concrete containing 1% steel fibers; it was 22.3 times greater than the one without fibers, with granodiorite aggregate. The concrete with 1% PF had an 11% higher mass loss than the one without PF. In the SC concrete, the increased amount and volume of capillary pores are the main causes of expansive internal pressure during the freezing of water. For the seven series of UHPC, the correlation between the percentage of mass decrease after the frost resistance test and the decrease/increase in mass after the salt crystallization resistance test is determined (Fig. 10).

This relationship can be described by the equation: $y = 0.00304x^2 - 0.0535x + 0.0832$. The polynomial trend was characterized by a good correlation coefficient $R^2 = 0.8322$ and relatively low errors in the intercept. It was observed that the results for UHPC with the highest SF content significantly differ from the other results as they have the highest mass loss in both the salt and frost resistance tests. It was observed that the addition of steel fibers appeared to decrease the internal material degradation due to the freeze–thaw cycles (Cwirzen et al. 2008). The experimental results showed that the weight loss of UHPC subjected to cycles of freezing and thawing in water was higher than the weight loss of UHPC after the salt crystallization resistance test. Steel fibers can have a major influence on

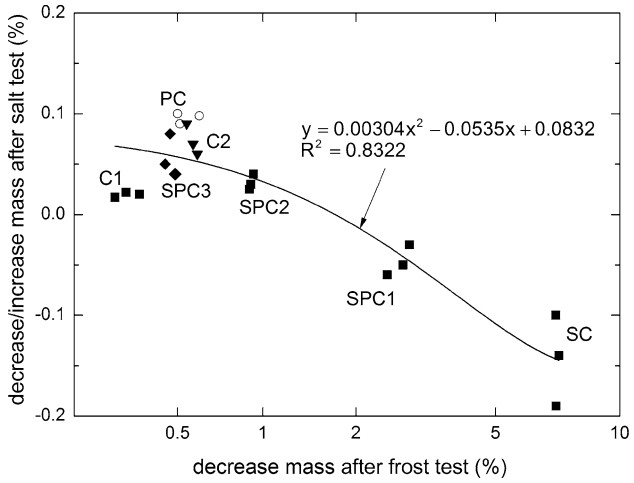

Fig. 10 Relationship between percentage of mass loss after frost and salt resistance tests.

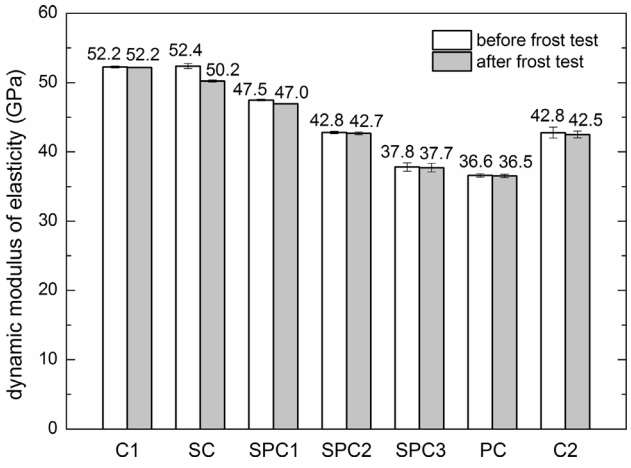

Fig. 11 Dynamic modulus of elasticity before and after freeze–thaw cycles.

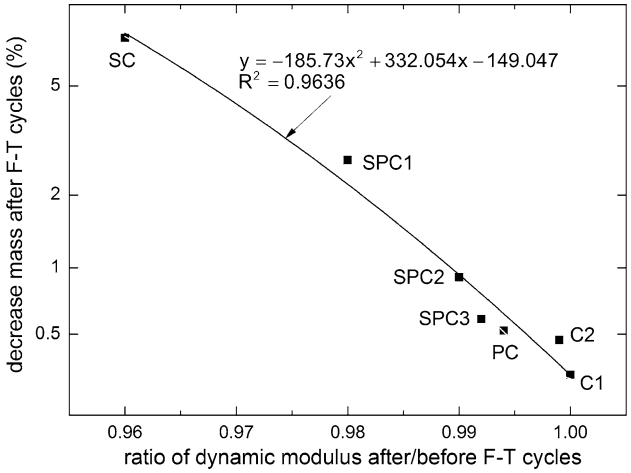

Fig. 12 Relationship between mass loss and dynamic modulus ratio after/before F–T cycles.

workability; one special concern is their orientation. In steel fiber reinforced concrete a well-finished sample surface helps encapsulate the fibers within the mortar. Material degradation due to freeze–thaw exposure can be caused by an imprecise finish of the sample surface and dense distribution of steel fibers near the outer edge of the samples. Furthermore, this may also be related to the differences in the physical properties of the frozen water and the salt solution such as freezing point, deformability or ductility (Miao et al. 2002). In this study, the steel fibers did not delay the onset or spread of micro-cracks, and thus do not protect against concrete degradation during cycles of freezing and thawing. The steel fibres are protected against corrosion in the alkaline environment of concrete, nevertheless, single fibres may corrode in the presence of moisture in the edge zone of the concrete samples. This corrosion caused significant failure and visual imperfections in the form of rust stains on the surface of UHPC with a content of at least 0.75% steel fibers (see Fig. 8). On the other hand, due to the extremely low porosity of UHPC compared to ordinary concrete and even high strength concrete, the rate of degradation is much slower and leads to significantly greater durability. The pores of UHPC are very fine and discontinuous and reduce the flow of reactive agents within the material, hence leading to limited material deterioration (Chemrouk 2015).

3.4 Dynamic Modulus of Elasticity After Frost Resistance Test

Dynamic modulus is important to evaluate the load bearing capacity of fiber reinforced UHPC, whose value is also a measure of frost resistance. Based on the theory of resonance, the frequencies of the concrete specimens before and after freezing-thawing cycles were measured. The results of the dynamic modulus of elasticity before and after the freeze–thaw cycles are presented in Fig. 11.

The highest dynamic modulus was displayed by the concrete with 1% SF, and is 27% higher than that of the concrete with 1% PF. After 180 freezing-thawing cycles, decreases in the dynamic modulus values were observed: 0.1% for C1, 4% for SC, 1% for SPC1, 0.3% for SPC2, 0.2% for SPC3 and 0.6% for C2. For all the mixtures the relative values of the dynamic elastic modulus do not drop below 95% of the baseline. Based on the above observation, it was found that all the examined UHPC are frost resistant. It was noted that the decreases in the dynamic modulus of elasticity are in close relationship with the mass losses for all types of UHPC. The correlations between the mass loss and the ratio of dynamic modulus before and after freezing and thawing (F–T) cycles were determined, (see Fig. 12).

The relationship between the loss in mass after the F–T cycles and the dynamic modulus of elasticity ratio is presented in the form of the polynomial $ax^2 + bx + c$. The high correlation coefficient value of more than 0.9636 indicates that the loss in mass has a strong relation to the ratio of the dynamic modulus of elasticity before and after F–T cycles. There is a clear grouping of the results depending on the type and quantity of fibers in UHPC, which was also observed in the relationship between the percentage of mass loss after the frost resistance test and after the salt resistance test (Fig. 10). The lowest results were noticed for the UHPC without fibers and with 1% PF. Conversely, the highest values were observed for the UHPC

with SF (Fig. 12). The middle part of the curve are the data obtained for the hybrid fiber reinforced UHPC.

3.5 Contact Angle and Surface Free Energy

Measuring the contact angle is one of the methods of monitoring changes in the wettability of the material surface. Surface free energy is often used as a measure of adhesive properties. The contact angle and SFE enable forecasting of material surface durability.

The measured contact angles of distilled water and the calculated SFE of UHPC after 0 and 35 min are included in Table 4. The contact angle before the frost resistance test after 0 and 35 min, and the contact angle before and after 180 F–T cycles at the beginning of the drop test are shown in Figs. 13 and 14 respectively.

It can be noticed that the distilled water contact angles (θ_w) decreased in the course of time and they are different before and after 180 F-T cycles. Decreases in the contact angle between 0 and 35 min after the frost resistance test were observed: 40.8° (C1), 34.8° (SC), 16.5° (SPC1), 28.4° (SPC2), 31.3° (SPC3), 31.9° (PC), 45.5° (C2). The contact angles after the frost resistance test after 0 min were high for the concrete without fibers and with steel fibers. Therefore, these UHPC were characterized by the lowest initial surface wettability. The hybrid fiber reinforced concrete and the polypropylene fiber reinforced concrete were characterized by initial wettability by up to 100% higher, except for the concrete with 0.25% SF and 0.75% PF (but in this case a smooth surface can lead to a higher value of contact angle). The highest contact angle was noted for the concrete with 1% SF both at the beginning of the test and after 35 min. The smallest contact angle was obtained by the concrete with the addition of 0.75% SF and 0.25% PF, which was about 38% lower than in the case of the concrete without fibers with the same granodiorite aggregate at the beginning of the experiment. These samples exhibited the greatest mass loss. Due to the corrosion of steel fibers on the concrete surface, the wettability and adhesion properties increased. The contact angle decreased by about 18% for the concrete with 1% SF and 13% for the concrete with 1% PF, whereas for the concretes without fibers, the contact angle decreased by about 5–6%. The contact angles after the frost resistance test after 35 min were high for the hybrid fiber reinforced concrete and polypropylene fiber reinforced concrete. The concretes with hybrid fibers had the least wettable surface of fiber reinforced concretes. The lowest contact angle was observed for the concrete without fibers with granite aggregate. This contact angle was about twice lower than that of the concrete without fibers with granodiorite aggregate. The absorptivity of coarse aggregate had an impact on the contact angle.

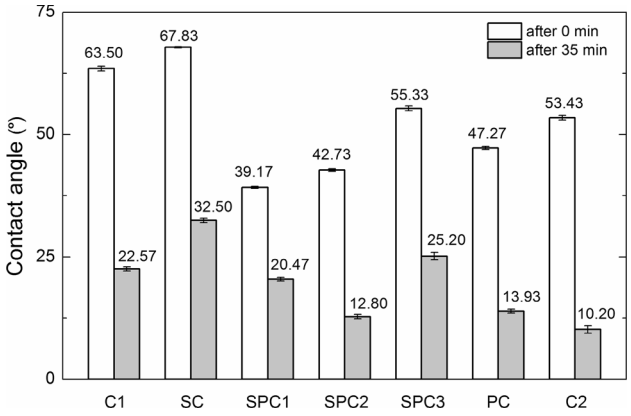

Fig. 13 Contact angle before F–T cycles after 0 and 35 min.

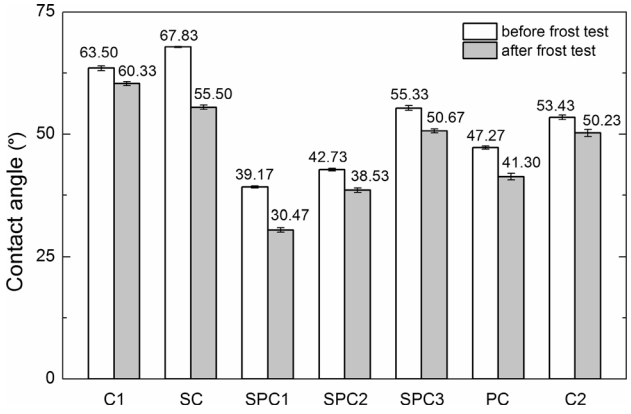

Fig. 14 Contact angle before and after 180 F–T cycles at beginning of drop test.

Table 4 UHPC contact angle and SFE.

Type of UHPC	Contact angle θ_w (°)				SFE γ_S (mJ/m^2)			
	Before frost test		After frost test		Before frost test		After frost test	
	$t_1 = 0$	$t_2 = 35$	$t_1 = 0$	$t_2 = 35$	$t_1 = 0$	$t_2 = 35$	$t_1 = 0$	$t_2 = 35$
	(min)							
C1	63.5	22.6	60.2	19.4	45.6	67.6	46.1	69.0
SC	67.8	32.4	55.4	20.6	43.1	63.3	50.6	68.5
SPC1	39.1	20.4	30.4	13.9	59.7	68.7	66.3	70.8
SPC2	42.7	12.9	38.5	10.1	58.1	71.1	62.2	71.7
SPC3	55.1	25.1	50.8	19.5	50.5	67.0	53.0	68.9
PC	47.2	14.0	41.2	9.3	55.4	70.6	57.7	71.9
C2	53.4	10.1	50.2	4.7	51.8	71.5	52.7	72.6

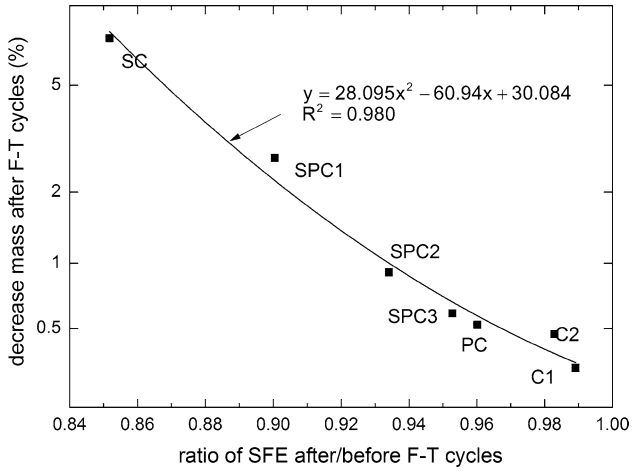

Fig. 15 Correlations between mass loss and SFE ratio before and after F–T cycles.

The total SFE values for all the UHPC were calculated (see Table 4). The highest SFE value $\gamma_S = 59.7$ mJ/m^2, which shows the finest adhesion properties, was obtained by the hybrid fiber reinforced UHPC with 0.75% SF and 0.25% PF. After the frost resistance test, all the SFE values were higher than before the test. The results were interpreted on the basis of the SFE ratio before and after F–T cycles. For the all the types of UHPC, the correlation between the mass loss and SFE ratio before and after the frost resistance test was determined (Fig. 15).

This relationship can be described by the equation $y = 28.095x^2 - 60.94x + 30.084$. The polynomial trend was characterized by an excellent coefficient $R^2 = 0.98$ and quite low errors in the intercept. The results for the concrete with the highest SF content were significantly different from the other results. They have the highest mass loss in the frost resistance test and the highest differences between SFE before and after the test.

4. Conclusions

Studies were performed to determine the impact of fiber hybridization on the salt crystallization resistance, the freeze–thaw resistance and the surface wettability of ultra-high performance concrete. Through careful analysis of the test results, the following conclusions can be drawn:

- The degree of ice pore saturation is sufficiently low. The matrices of the UHPC with steel fibers in the amounts of 1% (SC), and 0.75% (SPC1) are slightly damaged. The increased volume of free pores in UHPC with polypropylene fibers affected the greatest rise in mass after the salt crystallization test. All the UHPC exhibited good resistance to salt crystallization.
- Freezing-thawing cycles cause cracking and degradation of the UHPC with the high content of steel fibers, affecting deterioration of the dynamic modulus and significant loss in mass, which influences the durability. However, for all the UHPC the relative values of the dynamic elastic modulus do not drop below 95% of the baseline.
- The contact angles after the frost resistance test were high for hybrid fiber reinforced UHPC and polypropylene fiber reinforced UHPC. The lowest contact angle was observed for the concrete without fibers with granite aggregate. The highest SFE value was obtained by the hybrid fiber reinforced UHPC with 0.75% SF and 0.25% PF (SPC1).
- Ultra-high performance concrete demonstrated good correlations between: the mass loss and the dynamic modulus ratio before and after F–T cycles, the water absorptivity and increase in mass after the salt crystallization test, the percentage of mass loss after the frost resistance test and salt resistance test. The adhesive properties and wettability were determined by the correlation between the mass loss and SFE ratio before and after the F–T cycles.
- Fiber hybridization increases the resistance to salt crystallization and freeze–thaw resistance, improves the adhesion properties and reduce the wettability of the UHPC surface in comparison with one type of fiber at the same fiber volume fraction.

Acknowledgements

This work was financially supported by Ministry of Science and Higher Education—Poland, within the statutory research number S/15/B/1/2016, S/14/2016.

Open Access

References

Abbas, S., Nehdi, M. L., & Saleem, M. A. (2016). Ultra-high performance concrete: Mechanical performance, durability, sustainability and implementation challenges. *International Journal of Concrete Structures and Materials, 10*(3), 271–295.

Abdallah, S., Fan, M., Zhou, X., & Le Geyt, S. (2016). Anchorage effects of various steel fibre architectures for concrete reinforcement. *International Journal of Concrete Structures and Materials, 10*(3), 325–335.

Abou El-Mal, H. S. S., Sherbini, A. S., & Sallam, H. E. M. (2015). Mode II fracture toughness of hybrid FRCs. *International Journal of Concrete Structures and Materials, 9*(4), 475–486.

Afroughsabet, V., & Ozbakkaloglu, T. (2015). Mechanical and durability properties of high-strength concrete containing steel and polypropylene fibers. *Construction and Building Materials, 94,* 73–82.

Afroughsabet, V., Biolzi, L., & Ozbakkaloglu, T. (2016). High-performance fiber-reinforced concrete: A review. *Journal of Materials Science, 51,* 1–35. doi:10.1007/s10853-016-9917-4.

Aïtcin, P. C. (2003). The durability characteristics of high performance concrete: A review. *Cement & Concrete Composites, 25,* 409–420.

Barnat-Hunek, D., & Smarzewski, P. (2016). Influence of hydrophobisation on surface free energy of hybrid fiber reinforced ultra-high performance concrete. *Construction and Building Materials, 102,* 367–377.

Bencardino, F., Rizzuti, L., Spadea, G., & Swamy, R. N. (2010). Experimental evaluation of fiber reinforced concrete fracture properties. *Composites Part B: Engineering, 41*(1), 17–24.

Bondar, D., Lynsdale, C. J., Milestone, N. B., & Hassani, N. (2015). Sulfate resistance of alkali activated pozzolans. *International Journal of Concrete Structures and Materials, 9*(2), 145–158.

Çavdar, A. (2014). Investigation of freeze-thaw effects on mechanical properties of fiber reinforced cement mortars. *Composites Part B: Engineering, 58,* 463–472.

Chemrouk, M. (2015). The deteriorations of reinforced concrete and the option of high performances reinforced concrete. *The 5th International Conference of Euro Asia Civil Engineering Forum (EACEF-5). Procedia Engineering, 125,* 713–724.

Chemrouk, M., & Hamrat, M. (2002). High performance concrete—experimental studies of the material. *Proceedings of International Congress: Challenges of Concrete Construction, Conference 1: Innovations and Developments in Concrete Construction, Dundee, Scotland* (pp. 869–877).

Colombo, I. G., Colombo, M., & Di Prisco, M. (2015). Tensile behavior of textile reinforced concrete subjected to freezing-thawing cycles in un-cracked and cracked regimes. *Cement and Concrete Research, 73,* 169–183.

Cwirzen, A., Penttala, V., & Cwirzen, K. (2008). The effect of heat treatment on the salt freeze-thaw durability of UHSC. In *Proceedings of the 2nd International Symposium on Ultra High Performance Concrete*, *Kassel*, *Germany* (pp. 221–230).

Dawood, E. T., & Ramli, M. (2010). Development of high strength flowable mortar with hybrid fiber. *Construction and Building Materials, 24*(6), 1043–1050.

Dils, J., & De Schutter, G. (2015). Vacuum mixing technology to improve the mechanical properties of ultra-high performance concrete. *Materials and Structures, 48*(11), 3485–3501.

Dils, J., Boel, V., & De Schutter, G. (2013). Influence of cement type and mixing pressure on air content, rheology and mechanical properties of UHPC. *Construction and Building Materials, 41,* 455–463.

Dinh, N.-H., Choi, K.-K., & Kim, H.-S. (2016). Mechanical properties and modeling of amorphous metallic fiber-reinforced concrete in compression. *International Journal of Concrete Structures and Materials, 10*(2), 221–236.

Guse, U., & Hilsdorf, H. K. (1998). *Dauerhaftigkeit hochfester Betone. Schriftenreihe des Deutschen Ausschusses für Stahlbeton* (Vol. 487). Berlin: Beuth Verlag.

Kang, S.-T., Lee, K.-S., Choi, J.-I., Lee, Y., Felekoğlu, B., & Lee, B. Y. (2016). Control of tensile behavior of ultra-high performance concrete through artificial flaws and fiber hybridization. *International Journal of Concrete Structures and Materials, 10*(S3), 33–41.

Khitab, A., Arshad, M. T., Hussain, N., Tariq, K., Ali, S. A., Kazmi, S. M. S., et al. (2013). Concrete reinforced with 0.1 vol% of different synthetic fibers. *Life Science Journal, 10*(12), 934–939.

Köksal, F., Altun, F., Yiğit, İ., & Şahin, Y. (2008). Combined effect of silica fume and steel fiber on the mechanical properties of high strength concretes. *Construction and Building Materials, 22*(8), 1874–1880.

Koniorczyk, M., Konca, P., & Gawin, D. (2013). Salt crystallization-induced damage of cement mortar microstructure investigated by multi-cycle mercury intrusion. In Van Mier, J. G. M., Ruiz, G., Andrade, C., Yu, R. C. & Zhang, X. X. (Eds.), *VIII International Conference on Fracture Mechanics of Concrete and Concrete Structures FraMCoS-8*.

Li, H., & Liu, G. (2016). Tensile properties of hybrid fiber-reinforced reactive powder concrete after exposure to elevated temperatures. *International Journal of Concrete Structures and Materials, 10*(1), 29–37.

Miao, Ch., Mu, R., Tian, Q., & Sun, W. (2002). Effect of sulfate solution on the frost resistance of concrete with and without steel fiber reinforcement. *Cement and Concrete Research, 32,* 31–34.

Nili, M., & Afroughsabet, V. (2012). Property assessment of steel-fibre reinforced concrete made with silica fume. *Construction and Building Materials, 28*(1), 664–669.

Pierard, J., & Cauberg, N. (2009). Evaluation of durability and cracking tendency of ultra-high performance concrete. *Creep, shrinkage and durability mechanics of concrete and concrete structures* (pp. 695–700). London: Taylor and Francis Group.

Scherer, G. W. (1999). Crystallization in pores. *Cement and Concrete Research, 29*(8), 1347–1358.

Sivakumar, A., & Santhanam, M. (2007). A quantitative study on the plastic shrinkage cracking in high strength hybrid fibre reinforced concrete. *Cement & Concrete Composites, 29*(7), 575–581.

Smarzewski, P., & Barnat-Hunek, D. (2013). Surface free energy of high performance concrete with addition of polypropylene fibers. *Composites Theory and Practice, 15*(1), 8–15.

Smarzewski, P., & Barnat-Hunek, D. (2015). Fracture properties of plain and steel-polypropylene-fiber-reinforced high-performance concrete. *Materials and technology, 49*(4), 563–571.

Song, P. S., Hwang, S., & Sheu, B. C. (2005). Strength properties of nylon- and polypropylene-fiber-reinforced concretes. *Cement and Concrete Research, 35*(8), 1546–1550.

Sorensen, C., Berge, E., & Nikolaisen, E. B. (2014). Investigation of fiber distribution in concrete batches discharged from ready-mix truck. *International Journal of Concrete Structures and Materials, 8*(4), 279–287.

Structural Concrete. (2009). Textbook on behaviour, design and performance, Second edition, Volume 1, fib Bull.51.

Toutanji, H. A. (1999). Properties of polypropylene fiber reinforced silica fume expansive-cement concrete. *Construction and Building Materials, 13*(4), 171–177.

Wang, R., & Gao, X. (2016). Relationship between flowability, entrapped air content and strength of UHPC mixtures containing different dosage of steel fiber. *Applied Sciences, 6*(8), 216.

Wille, K., Naaman, A., & Montesinos, G. (2011). Ultra-high performance concrete with compressive strength exceeding 150 MPa (22 ksi): A simpler way. *ACI Materials Journal, 108*(1), 46–54.

Yang, K. H. (2011). Test on concrete reinforced with hybrid or monolithic steel and polyvinyl alcohol fibers. *ACI Materials Journal, 108*(6), 664–672.

Yang, H., Shen, X., Rao, M., Li, X., & Wang, X. (2015). Influence of alternation of sulfate attack and freeze–thaw on microstructure of concrete. *Advances in Materials Science and Engineering, 10,* 859069.

Yao, W., Li, J., & Wu, K. (2003). Mechanical properties of hybrid fiber-reinforced concrete at low fiber volume fraction. *Cement and Concrete Research, 33*(1), 27–30.

Yun, Y., & Wu, Y. F. (2011). Durability of CFRP-concrete joints under freeze-thaw cycling. *Cold Regions Science and Technology, 65*(3), 401–412.